LAWRENCE
LIVERMORE
NATIONAL
LABORATORY

LLNL-CONF-672905

Divertor Detachment Studies in DIII-D

D. N. Hill, A. G. McLean, A. W. Leonard, S. L. Allen, A. R. Briesemeister, B. M. Covele, M. Groth, M. A. Makowski, T. W. Petrie, V. A. Soukhanovskii, H. Y. Guo

June 11, 2015

European Physical Society
Lisbon, Portugal
June 22, 2015 through June 26, 2015

Disclaimer

Divertor Detachment Studies in DIII-D*

D.N. Hill[1], A.G. McLean[1], A.W. Leonard[2], S.L. Allen[1], A.R. Briesemeister[3], B.M. Covele[4], M. Groth[5], M.A. Makowski[1], T.W. Petrie[2], V.A. Soukhanovskii[1], and H.Y. Guo[2]

[1]*Lawrence Livermore National Laboratory, 7000 East Ave, Livermore, CA 94550, USA*
[2]*General Atomics, PO Box 85608, San Diego, CA 92186-5608, USA*
[3]*Oak Ridge National Laboratory, Oak Ridge, TN 37831, USA*
[4]*University of Texas, Austin, TX 78712-1192, USA*
[5]*Alto University, FI-00076, AALTO, Finland*

ITER and future burning plasma experiments require significant radiative dissipation in the edge and divertor plasma to obtain acceptable peak surface heat flux and erosion rates ($T_{e,div}$ < 5eV). The role of scrape-off layer (SOL) transport, divertor geometry, and magnetic configuration in determining the conditions required to achieve such divertor detachment remain uncertain, but has large impact on design and operation of next-step devices. Recent experiments in DIII-D have systematically examined the onset of divertor detachment using a variety of magnetic configurations and new/upgraded diagnostics including divertor Thomson scattering to produce 2D maps of the electron density and temperature.

Detachment dynamics in DIII-D

Detachment onset in DIII-D ELMing H-mode discharges is marked by a drop in divertor temperature (T_e≤1 eV), heat flux, and pressure as density rises in response to deuterium gas puffing from either the divertor region or the plasma midplane. The divertor Thomson system provides routine measurement of sub-eV electron temperatures between ELMs across both divertor legs by slowly sweeping the radial location of the X-point during a single discharge; the data are then mapped onto a single representative equilibrium, as shown in Fig. 1. It is

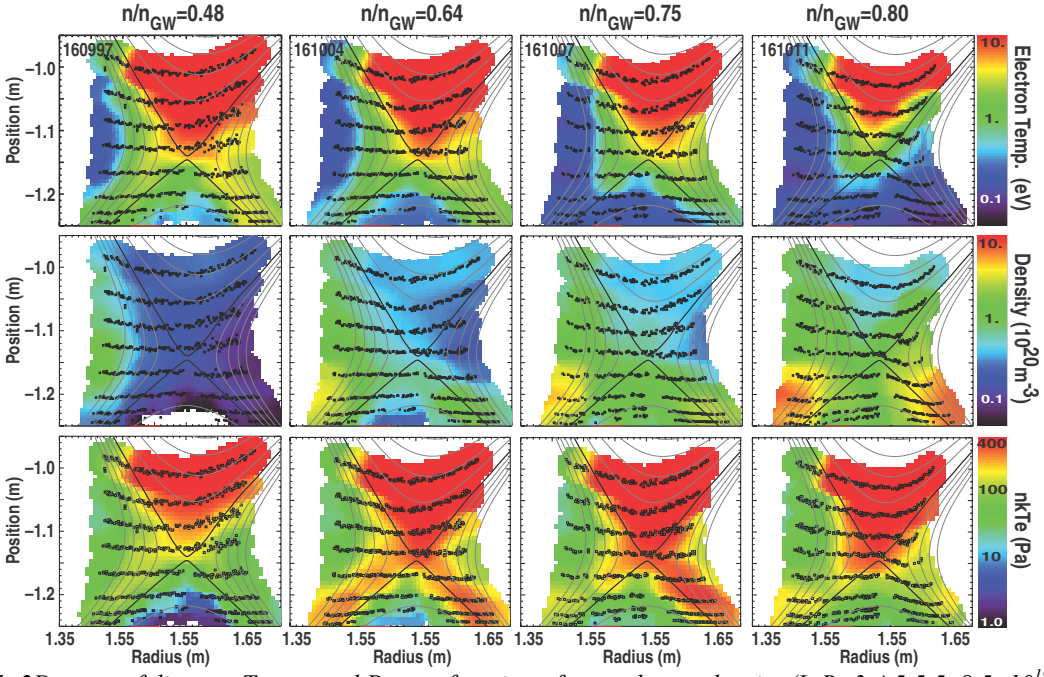

Fig. 1. 2D maps of divertor T_e, n_e, and P_e as a function of core plasma density (L-R: 3,4.5,5.5, 8.5×10^{19}m^{-3}

possible to systematically map the progression of detachment in DIII-D because it is highly reproducible and controllable for fixed core plasma conditions, and the relative openness of the lower divertor means that conditions are relatively independent of strike point location.

*This work was performed in part under the auspices of the U.S. Department of Energy by LLNL under DE-AC52-07NA27344, General Atomics under DE-FC02-04ER54698, and ORNL under DE-AC05-00OR22725.

Detachment in DIII-D begins first at the inner strike point, followed by the outer divertor at somewhat higher density, as shown in Fig. 1. Reversing B_{tor} significantly reduces the in/out detachment asymmetry by decreasing the relative density at the inner target as compared to the outer; the data appear qualitatively consistent with expectations based on $E \times B$ particle drifts[1] and quantitative analysis is now underway [2].

While measurements during ELMs are excluded from the data shown in this paper, they undoubtedly affect the overall divertor equilibrium, largely through their impact on global particle balance due to finite recycling times. For fixed shape, ELM frequency increases with power and with gas puffing; typical rates are ~100Hz for the discharges analysed here.

We focus our analysis of the detachment threshold in this and following sections on the two essential features most beneficial to fusion energy development: reduction of both peak heat flux and electron temperature at the divertor targets. The variation of peak divertor heat flux (q_{div}), electron temperature, density, and static electron pressure ($n_e \times T_e$) as a function of line-average core density is shown in Fig. 2, using data from the same discharges as the radial sweeps in Fig. 1 (I_p=0.9MA, B_t=-1.75T, P_{beam}=3.7MW). The ion saturation current as measured by a divertor Langmuir probe near the outer strike point and total radiative loss along the outer leg (determined from 2D reconstruction of bolometer data) are also shown.

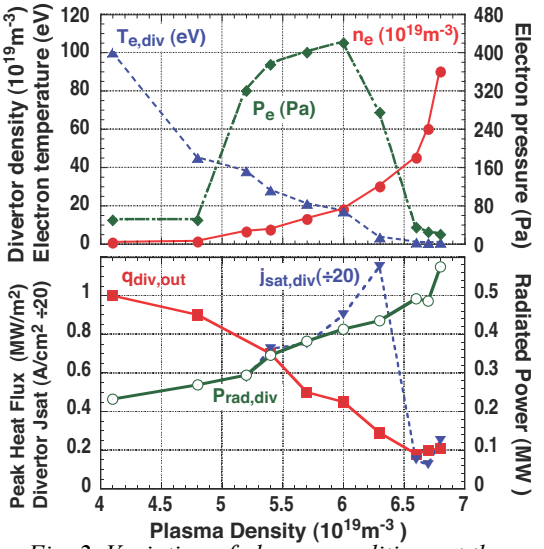

Fig. 2. Variation of plasma conditions at the outer divertor during a multi-shot density scan.

The outer leg strike point data in Fig. 2 span a wide range of divertor operating regimes. Below $\bar{n}_e \approx 4.5-4.8\times10^{19}\,m^{-3}$, $n_{e,target}$ in both divertors is low and $T_{e,target}$ is high. With increasing density, high recycling is established at the inner target, increasing n_e and sharply reducing T_e at both divertor targets. With density between $4.8-5.2\times10^{19}\,m^{-3}$, high recycling is established at the outer target and static electron pressure increases dramatically. With further gas puffing the divertor density and radiative loss continue rising as Te and divertor heat flux fall while pressure balance is preserved. Above $\bar{n}_e \approx 6\times10^{19}\,m^{-3}$ ($n_{e,div} > 20\times10^{19}\,m^{-3}$), pressure begins to fall and finally, when Te drops below 3eV near the target, the ion flux drops significantly – the plasma is detached from the outer target. At this time, the radiative loss is peaked in the outer SOL near the X-point and there is only a small change (~10-15%) in confinement, $n_{e,ped}$, $n_{e,sep}$, $T_{e,sep}$, or $\lambda_{Te,mp}$. Careful analysis of $\nabla T_{e,\parallel}$ and radiative emissivity along the outer divertor leg shows that ion convection dominates parallel heat transport in the detached state, extending the region over which impurity radiation can cool the plasma [3].

Detachment in Unit-recycling Helium Discharges without Carbon Radiation

Experiments in helium plasmas in DIII-D provide insight into detached divertor operation in future tokamaks with high temperature metal walls (no hydrocarbon formation and unit recycling). Helium operation in DIII-D eliminates chemical sputtering of carbon, increases ionization mean free paths in the divertor, reduces charge exchange and recombination rates compared to deuterium, and eliminates molecular-hydrogen effects.

Detachment experiments in L-mode helium plasmas with He-beam heating show that eliminating carbon as a significant radiator for divertor detachment does not increase the density for onset of detachment (remains ~0.6 of the Greenwald density limit). Bolometer measurements show very similar radiation profiles for the deuterium and helium plasmas, with the bulk of the radiation located in the divertor region. The peak emissivity is about 30%

higher and the total radiating volume is about twice as large in the helium plasma compared to a similar deuterium discharge. VUV spectroscopy shows that He^+ at 304Å is responsible for 90% of the radiation loss in the divertor, as compared to deuterium operation, where carbon is responsible for more than 50% of the radiation, mainly by CIV at 1550Å.

Even though the peak divertor heat flux drops by ~ a factor of 4 in these plasmas, the ion flux to the plate, as measured by Langmuir probes, does *not*, suggesting that volume recombination is not playing a significant role in the heat flux reduction. Thomson scattering data confirms that the electron temperature remains high enough to preclude significant volume recombination ($T_{e,div}$ > 2eV in He instead of < 1eV in deuterium). These data provide an important case study for analysis with 2D edge codes [4].

Detachment-Onset Threshold Studies

Our experiments show that the detachment threshold density depends most strongly on the SOL poloidal heat flux, q_{pol}, rather than parallel SOL heat flux ($q_{||}$). Whether *local* $q_{pol} = P_{SOL}/\lambda_q$ or $q_{||} = B_{tot}/B_{pol}\,\lambda_q$ governs divertor detachment is fundamental to developing approaches to manage peak divertor heat flux and target-plate sputtering in future tokamak fusion reactors because it drives significant design choices about the magnetic topology in the divertor. For example, the only way to reduce $q_{||}$ in the SOL is to either increase radial transport or major radius of the divertor leg; poloidal flux expansion does not reduce $q_{||}$. Clearly, parallel electron thermal transport dominates energy balance in the SOL adjacent to the confined plasma. In the divertor, however, the SOL plasma interacts with material surfaces and with recycled neutrals (fuel and impurities) through atomic physics processes. These interactions are independent of the field line geometry and can be both simultaneously localized in the poloidal dimension and broadly distributed in the parallel dimension along field lines.

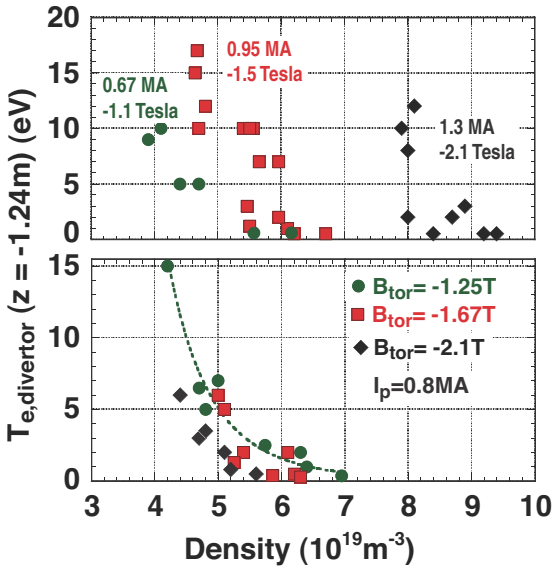

Fig.3. Divertor Te vs. plasma density. a) current scan at constant q95 (Btor ∝ Ip). b) toroidal field scan at constant plasma current.

To explore the relative importance of $q_{||}$ vs. q_{pol}, we varied q_{pol} through a series of power and current scans ($P_{sol} \propto P_{beam}$ and $\lambda_q \propto 1/I_p$), and parallel heat flux $q_{||}$ through a toroidal field scan at constant P_{sol} and λ_q ($q_{||} \propto B_{tor}$ at constant I_p) , results of which appear in Fig. 3. For the current scan, the toroidal field was varied in step with I_p to fix the field line pitch angle and parallel connection length. For the toroidal field scan, the plasma current was held fixed in order maintain constant midplane heat flux width and q_{pol}, which necessarily results in an increase of parallel connection length proportional to the change in B_{tor}. The data show that the line-average plasma density required to achieve detached conditions (i.e., $T_{e,div}$<5eV) increases significantly with the increase in q_{pol}, while the density at detachment onset actually *decreases* as $q_{||}$ doubles during the toroidal field scan. We speculate that increased field line length in the high neutral density region within a poloidal mean-free path of the divertor target significantly enhances energy dissipation through collisional excitation of fuel and impurity atoms, charge exchange, and pressure loss through volume recombination.

Divertor Configuration Studies

The effect of divertor geometry (poloidal length and magnetic flux expansion) was examined by varying the x-point to target-plate distance (δ_{pol}), and by operating with both

snowflake and X-divertor configurations. Increasing δ_{pol} by about a factor of three, from 0.2m to 0.5m, resulted in a strong reduction in peak target heat flux at high density as compared to a more divertor, even though poloidal flux expansion was reduced by a similar factor. The longer divertor leg at the outer strike point also increased the effectiveness of argon injection in reducing peak heat flux [5].

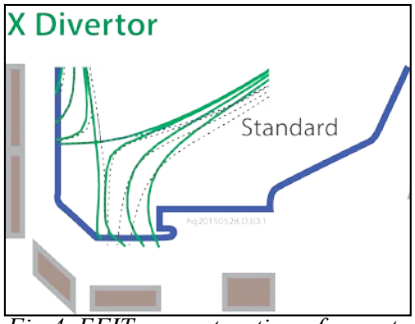

Fig.4. EFIT reconstruction of recent X-divertor configurations in DIII-D.

The effect of increasing poloidal flux expansion near the x-point and near the divertor targets was explored using exact Snowflake[6], Snowflake minus (SF–), and X-divertor configurations [7]. Naturally, the poloidal flux expansion reduced peak divertor heat flux in attached conditions by increasing the contact area by ~***TBD*** for the SF– configuration and ~ ***TBD*** for recent X-divertor discharges (shown in Fig. 4). In the SF– experiments, even the ELM heat pulses were suppressed [8].

Experiments are now being planned to explore the effect of divertor closure (use of shaped divertor structures to enhance neutral trapping near the divetor strike points). In the first phase, we will compare detachment onset density between the open lower divertor with the more closed upper divertor in DIII-D. SOLPS modeling suggests that further enhancement of the degree of divertor closure by small modifications to the shape of the upper divertor tiles may further reduce the detachment threshold density. Fig. 5 shows the concept for the upper divertor modification. The shaped-slot strongly reduces the divertor T_e and target heat flux by redirecting and confining recycling neutrals and impurities near the target. This may enable detachment onset at a lower upstream density than for a rectangular slot.

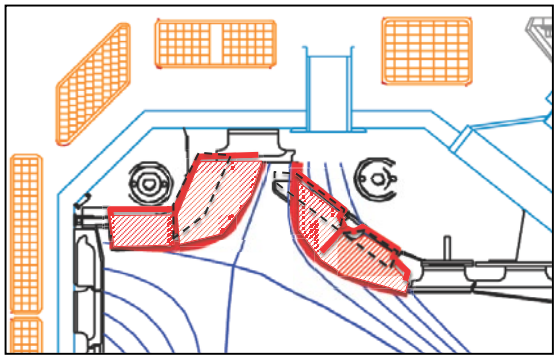
Fig.5. Overlay of conceptual layout for proposed upper-divertor tile modifications (red) in DIII-D.

Summary

The experiments described here seek to improve the physics basis for designing capable divertors for future burning plasma experiments. Focused variations in plasma parameters and divertor geometry, supported by a comprehensive set of divertor diagnostics, aim to test understanding and provide key data for direct comparison with edge simulation codes.

References

1. M. Groth, G.D. Porter, M.E. Rensink, *et al.*, J. Nucl. Mater. **415** (2011) S530.
2. A. McLean, in preparation.
3. A.W. Leonard, M.A. Mahdavi, C.J. Lasnier, *et al.*, Nucl. Fusion **52** (2012) 063015.
4. A. Loarte, A. Kukushkin, G.D. Porter, , et al., Contrib. Plasma Phys. **40** (2000) 508
5. T.W. Petrie, J.M. Canik, C.J. Lasnier, *et al.*, Nucl. Fusion **53** (2013) 113024.
6. D. Ryutov, Phys. Plasmas **14** (2007) 064502
7. P.M. Valanju, M. Kotschenreuther, *et al.*, Phys. Plasmas **16** (2009) 056110
8. D.N. Hill and the DIII-D Team, Nucl. Fusion 53 (2013) 104001.